

Electrochemical impedance of the cathode catalyst layer in polymer electrolyte fuel cells

M. Eikerling *, A.A. Kornyshev

Institute for Materials and Processes in Energy Systems, IWV-3, Research Center 'Jülich' GmbH, D-52425 Jülich, Germany

Received 22 March 1999; received in revised form 30 June 1999; accepted 30 July 1999

Abstract

A macrohomogeneous model that was studied in a previous publication under stationary conditions is used to calculate the small-signal dynamic response of the cathode catalyst layer in polymer electrolyte fuel cells. Within this approach the effects of reaction kinetics and double layer capacitance at the dispersed catalyst | electrolyte interface, proton conductivity of the electrolyte network within the layer and oxygen diffusion through the gas-pore space are studied. The analytical expressions derived reveal relationships between the structure of the layer and impedance spectra. Particularly strong dependences of the differential resistivity on the electrode composition appear if either proton transport or oxygen diffusion dominate the voltage losses. This happens for compositions that are close to the percolation thresholds of either proton conductivity in the electrolyte network or gas-pore diffusivity. Due to proton transport limitations, a linear branch is seen in impedance spectra in the high frequency limit, whereas in the low frequency domain a semicircular part arises. These results may help to distinguish the contribution of the catalyst layer from the contribution of other fuel cell components and characterize it quantitatively. © 1999 Elsevier Science S.A. All rights reserved.

Keywords: Polymer electrolyte fuel cell; Catalyst layer; Complex impedance

1. Introduction

Optimization of the structure and performance of porous composite electrodes for fuel cell applications is a challenging commitment, where electrochemistry, material science and electrical engineering meet [1–6]. The worldwide extending R&D-efforts are motivated by economical and ecological impacts of these rapidly developing energy conversion technologies. Essential characteristics of well-performing electrodes are a large active reaction zone for the electrochemical reaction and a good accessibility of the reaction sites to the reacting species.

In the case of polymer electrolyte fuel cells (PEFC) the cathodes give a significant, if not the major, contribution to the total efficiency losses due to the high overpotential of the oxygen reduction reaction (orr). Pt-catalyst particles are dispersed in the composite structure in order to obtain sufficient reaction rates at the typical working temperatures of ca. 90°C. A high utilization of the catalyst

can, however, only be attained if the cathode structure is impregnated with fractions of proton conducting material [7–9]. Recently, some efforts have been made towards the reduction of the Pt-amount, which is one of the major R&D goals in view of making PEFC competitive for commercialization. Excellent performance characteristics of PEFC-cathodes were already reported with Pt-loadings as low as 0.1 mg Pt cm⁻² by Gottesfeld et al. [5].

This report comprises several aspects of the structure function optimization of PEFC-cathodes and is an extension of previous work on the theory of polarization curves [10]. In Ref. [10] a macrohomogeneous model which includes (i) proton transport through the polymer–electrolyte network, spanning the sample; (ii) oxygen supply through a network of (hydrophobized) gas pores, and (iii) electrochemical reaction at the effective reaction surface, i.e. the catalyst | electrolyte interface, was explored. The model describes, how, due to limited supplies of oxygen and protons, the catalyst utilization varies with current density. Different regimes in which either the losses due to proton transport, reaction kinetics or limited oxygen supply prevail were revealed.

* Corresponding author. Fax: +49-2461-61-6695.

E-mail address: m.eikerling@fz-juelich.de (M. Eikerling)

In the present work this model is extended to describe the complex impedance of the cathode catalyst layer. It is shown that impedance spectroscopy can be used to determine electrode parameters as functions of the structure and composition. This helps to monitor changes of distinct electrode functionalities with the variation of different ingredients, and, therefore, to control the overall electrode performance.

The potential benefit of impedance studies of porous gas diffusion electrodes was identified earlier by Springer and Raistrick [11,12]. Consideration of the time dependence involved in double layer charging allowed resolution of different electrochemical processes. Here, the models are adjusted to take into account the specific environment of cathode catalyst layers in PEFC, and the effects of variable composition are studied explicitly by means of incorporation of percolation type dependences.

Several important aspects of catalyst utilization and specific effective surface area in porous electrodes have been studied earlier, e.g. by Mund et al. [13]. More recently, an excellent review of theory and models of current transformation in porous two- and three-phase electrodes was given in Ref. [14]. The basic mathematics used here are similar to those described in Ref. [14]. However, the derivation of analytical expressions presented here goes beyond the earlier approaches. Special emphasis is put on the calculation of complex impedance and the explicit study of frequency-dependent effects. Relations between fundamental parameters describing the properties of the layer and features in impedance spectra are derived. Furthermore, revelation of effects due to varying electrode composition provides diagnostic tools and means for optimization of the composition. Similar studies have been undertaken by Springer et al. [15]. They investigated experimentally and theoretically the impedance response of PEFC. Their method of solution is, however, entirely numerical. Moreover, composition dependent effects of catalyst layer performance in impedance spectra were not studied in Ref. [15].

2. The model and basic equations

The so-called ‘agglomerate structure model’ of the catalyst layer is depicted in Fig. 1 (a). The model representation is based on the agglomerates of carbon particles, bounded together by polytetrafluoroethylene (PTFE) which serves, in addition, as a hydrophobizing agent in order to ensure a good gas porosity of the layer. The voids between the agglomerates are penetrated by the polymer electrolyte, which forms the proton conducting pathways. Reaction acts take place at those catalyst particles which are in contact with both carbon and electrolyte phases.

As in Ref. [10] (see also Ref. [16]) the catalyst layer is treated as an effective homogeneous medium, whose

performance is characterized by a specific proton conductivity σ_p , an effective diffusion constant of oxygen supply D^0 and parameters for the interfacial charge transfer processes (Tafel-slope b and exchange current density i^*). Ohmic losses in the well-connected electronic conductor-phase are neglected, so that the carbon phase will be considered equipotential.

The system is studied under isothermal conditions. Only effects in the catalyst layer are considered. Experimentally it is possible to separate the catalyst layer processes from processes in the backing layer by making the latter very thin ($\sim 1 \mu\text{m}$, compared with catalyst layer thicknesses $\sim 10 \mu\text{m}$). Boundary conditions are fixed at the catalyst layer | backing layer interface. All the variables are assumed to depend only on the coordinate z (c.f. Fig. 1 (a)), so that mathematically the problem is unidimensional. This model was studied previously under stationary conditions [10]. Here it is extended to include dynamic charging processes of the electrical double layers in parallel to the Faradaic charge transfer processes, as represented by the transmission line shown in Fig. 1.

An essential element involved in the dynamic response is the capacitance of the double layer formed by H^+ or H_3O^+ at the interface of the charged catalyst or carbon particles and polymer electrolyte. The differential capacitance is generally a function of the local potential drop φ across the electrolyte | carbon interface. Assuming that this variation is small in the range of φ considered, it will be neglected.

The general model includes ohmic losses in the electrolyte, losses due to oxygen diffusion, interfacial charge transfer and double layer charging. The basic equations are:

$$\frac{\partial \varphi(z, t)}{\partial z} = -\frac{1}{\sigma} j(z, t), \quad \sigma = \frac{\sigma_p}{l} \quad (1)$$

$$\frac{\partial j(z, t)}{\partial z} = -J(z, t) - \mathcal{C}_{\text{dl}}(\varphi) \frac{\partial \varphi}{\partial t} \quad (2)$$

$$\frac{\partial p(z, t)}{\partial z} = \frac{j_0 - j(z, t)}{I}, \quad I = \frac{4FP_0D^0}{RTl}, \quad p = \frac{P}{P_0} \quad (3)$$

Eq. (3) implies Knudsen flow as the dominant mechanism of diffusion. φ is the local electrode potential, which is defined as the potential difference between electronic conductor phase and electrolyte¹. The dimensionless coordinate z is normalized to the thickness l of the layer. Since the electronic conductor is considered

¹ Note, that this definition of electrode potential, which is frequently termed ‘overpotential’ in the context of fuel cell research, deviates from the classical textbook-definition of overpotential, c.f. Vielstich [17]. In the latter reference, overpotential is defined as the difference between electrode potential and concentration-dependent Nernst-potential. The notions of electrode potential, as it is used here, and classically defined overpotential are equivalent only in the case when local variations in concentrations are negligible, which is e.g. realized in the limit of small electrode potentials.

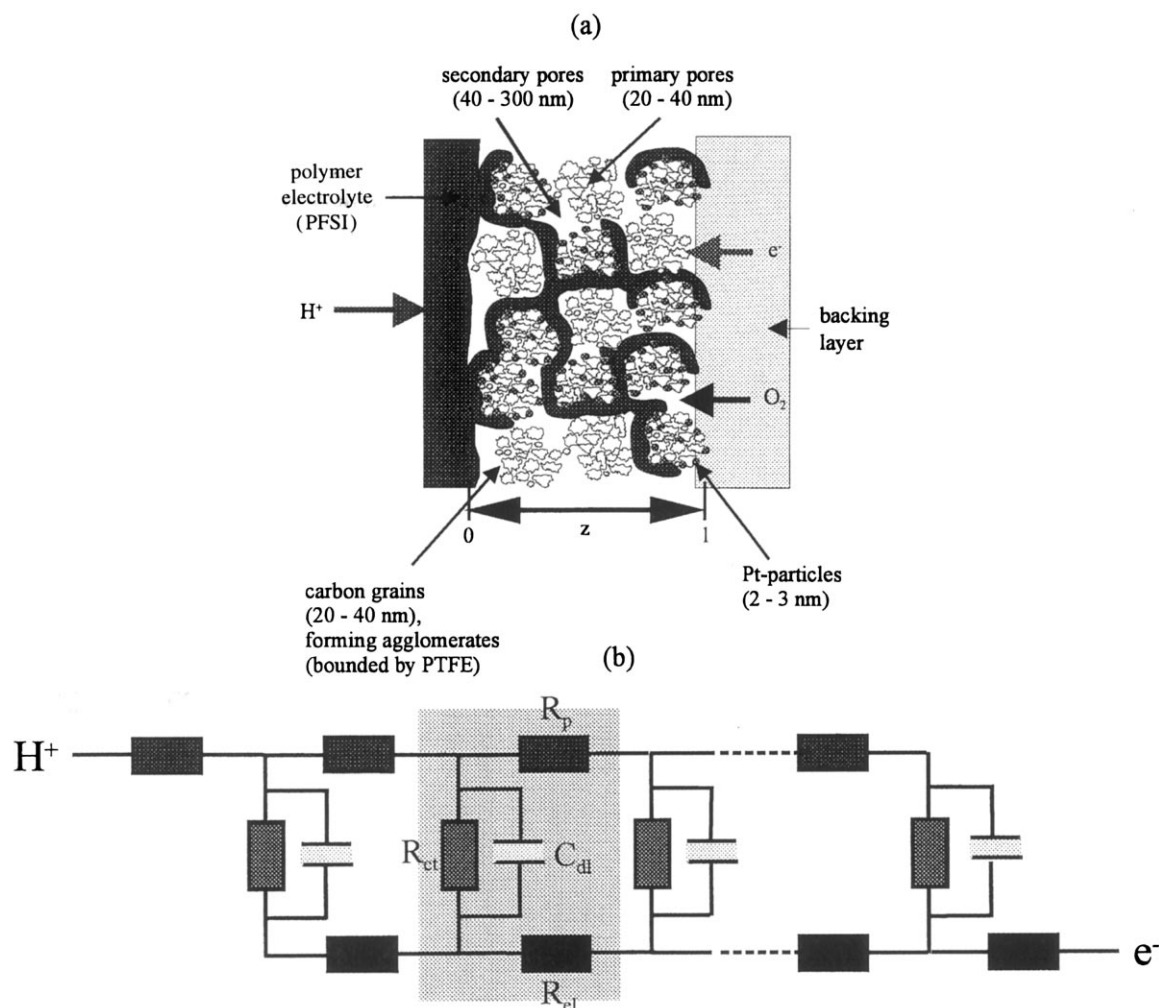


Fig. 1. Schematic picture of the catalyst layer geometry and its composition, exhibiting the different functional parts. (a) The sketch of the layer, used for the construction of the continuous model. (b) The one-dimensional transmission line equivalent circuit where the elementary unit with protonic resistivity R_p , charge transfer resistivity R_{ct} and double layer capacitance C_{dl} is highlighted.

to be equipotential, the drop in φ is equal to the potential drop in the electrolyte phase. Thus Eq. (1) is Ohm's law in the electrolyte phase. Eq. (2) is the continuity equation which describes the transformation of protonic current density j into electronic current via Faradaic processes (first term on the rhs) and the double layer charging in the time dependent electric fields (second term on the rhs).

The linear approximation

$$J(z, t) = \frac{2i^*}{b} \varphi(z, t) \quad (4)$$

gives the Faradaic current in the limit of small electrode potentials, $\varphi \lesssim b/3$, where b is the Tafel slope and i^* the exchange current density,

$$i^* = FS_0/k^*(c_{H^+})^{\nu}c_{O_2}^* \quad (5)$$

Here, F is Faraday's constant, S_0 the effective surface of the Pt | PFSI-contact area, and k^* the rate constant of the electrochemical reaction; c_{H^+} is the proton con-

centration in the electrolyte phase, which is assumed to be constant due to electroneutrality; $c_{O_2}^*$ is the concentration, with which oxygen is supplied at the catalyst layer | backing layer boundary. In the regime of high electrode potentials, $\varphi \gtrsim 2b$, the Faradaic current density can be approximated by the Tafel expression

$$J(z, t) = i^* \exp\left(\frac{\varphi(z, t)}{b}\right) \quad (6)$$

The double layer capacitance per unit of geometric surface area of the electrode, \mathcal{C}_{dl} , in Eq. (2) is given by

$$\mathcal{C}_{dl} = \varepsilon\varepsilon_0 \frac{S_{dl}l}{\delta} \quad (7)$$

This is based on a simple estimate that uses the plate capacitor formula. S_{dl} (in cm^2 per cm^3) is the specific surface of the electrolyte|metal (carbon and Pt) interface. δ is the thickness of the double layer and ε is the dielectric constant of the medium between the mobile protons in the electrolyte and the interface.

In this study the possible dependence of \mathcal{C}_{dl} on φ will be neglected. Concentrations of charge carriers in water filled pores are about 3 M solutions in the water bulk. This means that consideration of the so-called ‘lattice saturation effects’ may be essential (these do not allow a considerable accumulation of protons in the double layer upon its charging [18]). Under these conditions \mathcal{C}_{dl} does not show a significant φ -dependence.

In Eq. (3) P_0 is the partial pressure with which oxygen is supplied at $z = 1$. p is the local oxygen partial pressure, normalized to P_0 . D^0 is the diffusion constant of oxygen. T is the temperature and R is the universal gas constant.

3. The transmission line equivalent circuit

In Fig. 1 (b) we show a discretized transmission line with m elements (agglomerates), which mimics the continuous electrical network of the catalyst layer. Each element consists of a proton resistance (R_p), a charge transfer resistance (linear, R_{ct} , or non-linear and, thus, characterized by an apparent Tafel slope b and the exchange current density i^*) and an electron resistance (R_{el}) which, however, will be neglected, being small compared to other resistances. In addition to the obstacles against charge transport formed by these resistances double layer charging effects are represented by double layer capacitances C_{dl} in parallel to R_{ct} ².

The formalism for the calculation of current-voltage characteristics and complex impedance within the transmission-line framework is based on the Kirchhoff equations. If appropriate boundary conditions at the catalyst layer | backing layer interface ($j = 0$, $\varphi = \varphi_l$) are fixed then the output of performance (j_m , φ_m) after every subsequently added element (label m) in the direction towards the electrolyte is determined by iterative relations.

The transmission line equivalent circuit has a continuous limit of $m \rightarrow \infty$, in which the equations of the discrete model resemble the equations of the continuous model. Indeed, let us divide the catalyst layer into slices of thickness l_e . The parameters of the transmission line elements may then be related to the average macroscopic parameters of the catalyst layer:

$$R_p = \frac{l_e}{\sigma_p}, \quad R_{ct} = \frac{bl}{2i^*l_e}$$

For PEFC the following hierarchy between the three main resistances of the model is typical

$$R_{el} \ll R_p < R_{ct}$$

² Oxygen diffusion limitations are not shown in Fig. 1 (b). They can, however, be considered as well within the transmission line approach, introducing a line of discretized diffusion resistances in parallel to the proton transport resistances.

The double-layer capacitance of a transmission-line element is

$$C_{dl} = \epsilon \epsilon_0 \frac{S_{dl} l_e}{\delta} \quad (8)$$

4. Basic solution and limiting cases

In the stationary problem it is possible to obtain analytical solutions in certain limiting cases, when one of the transport processes causes only negligible losses. These approximate analytical solutions will also be used for the calculation of the dynamic response. In the first part of this section we consider the case when oxygen diffusion limitations are negligible, whereas in the second part they are allowed to be of equal importance as proton transport limitations. The interplay between the different limiting cases is controlled by the composition of the electrode and by the working regime.

4.1. Fast oxygen diffusion-stationary solution

The stationary problem has analytical solutions in the regime in which the effect of oxygen depletion can be neglected [10]. The same regime will be considered in the first part of the dynamic theory presented here. For the sake of completeness the stationary solution results which have been presented elsewhere before [10,16], are summarized here.

The boundary conditions for the stationary solution (superscript 0) are

$$j^0(z=1) = 0 \quad \text{and} \quad \varphi^0(z=1) = \varphi_l$$

The value of φ_l determines the proton current density j^0 that enters the cathode at its interface with the membrane.

In the *linear regime* (low overpotentials) the current-voltage characteristics are determined by

$$j^0(z) = j_0 \frac{\sinh\left(\frac{1}{\lambda_p}(1-z)\right)}{\sinh\left(\frac{1}{\lambda_p}\right)}$$

$$\varphi^0(z) = j_0 \sqrt{\frac{b}{2i^*\sigma}} \frac{\cosh\left(\frac{1}{\lambda_p}(1-z)\right)}{\sinh\left(\frac{1}{\lambda_p}\right)} \quad (9)$$

where we introduced a notion of the reaction-penetration depth

$$\lambda_p = \sqrt{\frac{\sigma b}{2i^*}} l \equiv \sqrt{\frac{R_{ct}}{R_p}} l_e \quad (10)$$

The electrode polarization resistance is, thus,

$$R = \frac{\varphi^0(0)}{j^0(0)} = \sqrt{\frac{b}{2i^*\sigma}} \coth\left(\frac{l}{\lambda_p}\right) = \sqrt{R_p R_{ct}} \coth\left(\frac{l}{\lambda_p}\right) \quad (11)$$

In the *nonlinear regime*, where Tafel kinetics apply, the stationary solution takes a parametric form [10]:

$$j^0(z) = 2\sigma b \zeta \tan(\zeta(1-z))$$

$$\varphi^0(z) = 2b \ln \left\{ \frac{2\lambda_p \zeta}{\cos(\zeta(1-z))} \right\} \quad (12)$$

where

$$\zeta = \sqrt{\frac{i^*}{2\sigma b}} \exp\left(\frac{\varphi_l}{2b}\right)$$

Correspondingly the differential resistivity of the electrode is given by

$$R_{\text{diff}} = \frac{d\varphi^0(0)}{dj^0(0)} = 2R_{\text{ct}} \exp\left(-\frac{\varphi_l}{b}\right) \frac{l_e}{l} f(\zeta)$$

$$f(\zeta) = 2\zeta \frac{\cos^2(\zeta) + \zeta \sin(\zeta) \cos(\zeta)}{\zeta + \sin(\zeta) \cos(\zeta)} \quad (13)$$

4.2. Dynamic response

In this subsection a small dynamic potential perturbation is considered, which is applied at $z=1$. The boundary conditions are fixed in the following way: since we calculate the linear response to a small time-dependent signal, superimposed on the bias potential at the working point, the impedance will not depend on the perturbation potential. The absolute value of the latter should be small compared to b . As in the stationary case, the dynamic current signal at $z=1$ is zero, i.e. $\delta j_l = 0$, since no protons are allowed to pass this interface.

4.2.1. Linear regime

Complex impedance in the small electrode potential regime is given by:

$$Z = \frac{\varphi^0(0)}{j^0(0)} = \sqrt{R_p Z_{\text{ct}}} \coth\left(\sqrt{\frac{R_p}{Z_{\text{ct}}}} \frac{l}{l_e}\right)$$

$$Z_{\text{ct}} = \frac{R_{\text{ct}}}{1 + i \frac{\omega}{\omega_c}} \quad (14)$$

similar to the stationary solution, but with R_{ct} replaced by Z_{ct} . Here, $i = \sqrt{-1}$, ω is the frequency of the sinusoidal perturbation, and ω_c the characteristic frequency,

$$\omega_c = \frac{2i^* \delta}{\epsilon \epsilon_0 b l S_{\text{dl}}} = \frac{1}{R_{\text{ct}} C_{\text{dl}}} \quad (15)$$

The frequency-dependent complex impedance is

$$Z(\omega) = \sqrt{R_p R_{\text{ct}}} \frac{\exp\left(-i \frac{\phi}{2}\right)}{\left(1 + \frac{\omega^2}{\omega_c^2}\right)^{1/4}}$$

$$\frac{\cosh\left(\kappa \cos \frac{\phi}{2}\right) \sinh\left(\kappa \cos \frac{\phi}{2}\right) - i \cos\left(\kappa \cos \frac{\phi}{2}\right) \sin\left(\kappa \cos \frac{\phi}{2}\right)}{\sin^2\left(\kappa \sin \frac{\phi}{2}\right) + \sinh^2\left(\kappa \cos \frac{\phi}{2}\right)} \quad (16)$$

with

$$\phi = \arctan \frac{\omega}{\omega_c} \quad \text{and} \quad \kappa = \frac{l}{\lambda_p} \left(1 + \frac{\omega^2}{\omega_c^2}\right)^{1/4}$$

4.2.2. Tafel regime

In order to calculate the dynamic response to a small perturbation ($\delta\varphi$, δj) at the working point (φ^0 , j^0) the complex signals are split into their stationary and dynamic parts in Fourier-space,

$$\varphi(z, \omega) = \varphi^0(z) + \delta\varphi(z, \omega) \quad \text{and} \quad j(z, \omega) = j^0(z) + \delta j(z, \omega) \quad (17)$$

For $\delta\varphi/b \ll 1$ ($b \approx 30-50$ mV),

$$\exp\left(\frac{\varphi}{b}\right) = \exp\left(\frac{\varphi^0 + \delta\varphi}{b}\right) \approx \exp\left(\frac{\varphi^0}{b}\right) \left(1 + \frac{\delta\varphi}{b}\right) \quad (18)$$

The working regime is specified by the value of $\varphi^0(z=l) \equiv \varphi_l$, which determines the stationary solution $j^0(z)$, $\varphi^0(z)$ (Eq. (12)) and the corresponding differential resistivity (Eq. (13)).

This stationary solution is used in the Fourier transforms of Eqs. (1) and (2). Subtracting the stationary parts from these equations gives equations on the dynamic response,

$$\frac{d(\delta\varphi)}{dz} = -\frac{1}{\sigma} (\delta j),$$

$$\frac{d(\delta j)}{dz} = -\left(\frac{i^*}{b} \exp\left(\frac{\varphi^0(z)}{b}\right) + i\omega \mathcal{C}_{\text{dl}}\right) (\delta\varphi) \quad (19)$$

Upon the substitution of $\varphi^0(z)$, given by Eq. (12) into Eq. (19) we obtain

$$\frac{d^2(\delta\varphi)}{dz^2} = \frac{l^2}{\tilde{\lambda}_p^2(\varphi_l)} \left(\frac{1}{\cos^2(\zeta(1-z))} + i \frac{\omega}{\tilde{\omega}_c(\varphi_l)}\right) (\delta\varphi) \quad (20)$$

Here, we have used the following definitions

$$\tilde{\lambda}_p(\varphi_l) = \sqrt{2} \lambda_p \exp\left(-\frac{\varphi_l}{2b}\right)$$

$$\tilde{\omega}_c(\varphi_l) = \frac{1}{2} \omega_c \exp\left(\frac{\varphi_l}{b}\right) \quad (21)$$

The boundary conditions to Eq. (20) are again fixed at $z=1$, where $\delta\varphi$ is given some small arbitrary value $\delta\varphi_l$. As the response is considered to be linear to a small perturbation, $\delta\varphi_l \ll b$, the differential impedance does not depend on $\delta\varphi_l$. The second boundary condition is $(d(\delta\varphi)/dz)_{z=1} = 0$, since no ionic current, either dc or ac, is allowed to cross the boundary with the backing layer.

A simple solution can be obtained when $\tilde{\lambda}_p$ is large compared to the thickness of the electrode. Indeed, for this case the variation of $\varphi_0(z)$ with z can be neglected, i.e. the electrolyte phase in the electrode is equipotential, and Eq. (20) reduces to

$$\frac{d^2(\delta\varphi)}{dz^2} = \frac{l^2}{\tilde{\lambda}_p(\varphi_l)^2} \left(1 + i \frac{\omega}{\tilde{\omega}_c(\varphi_l)} \right) (\delta\varphi) \quad (22)$$

In this case the dynamic response of the catalyst layer in the Tafel regime is the same as in the linear regime, however with the renormalized penetration depth $\tilde{\lambda}_p$ and characteristic frequency $\tilde{\omega}_c$. Due to the exponential acceleration of the reaction rate with electrode potential, the penetration depth decreases and the characteristic frequency increases exponentially.

The variation of $\varphi^0(z)$ is small ($\lesssim 5\%$) as long as $\tilde{\lambda}_p > 2l$. Therefore, as a practical criterion for the applicability of Eq. (22), we may use inequality

$$2b < \varphi_l < 2b \ln\left(\frac{\lambda_p}{\sqrt{2l}}\right) \quad (23)$$

where the lower boundary signifies the validity of the Tafel kinetics. Within this overpotential interval.

$$Z(\omega) = \sqrt{2R_p R_{ct}} \exp\left(-\frac{\varphi_l}{2b}\right) \frac{\exp\left(-\frac{\tilde{\varphi}}{2}\right)}{\left(1 + \frac{\omega^2}{\tilde{\omega}_c^2}\right)^{1/4}}$$

$$\frac{\cosh\left(\tilde{\kappa} \cos \frac{\tilde{\varphi}}{2}\right) \sinh\left(\tilde{\kappa} \cos \frac{\tilde{\varphi}}{2}\right) - i \cos\left(\tilde{\kappa} \cos \frac{\tilde{\varphi}}{2}\right) \sin\left(\tilde{\kappa} \cos \frac{\tilde{\varphi}}{2}\right)}{\sin^2\left(\tilde{\kappa} \cos \frac{\tilde{\varphi}}{2}\right) + \sinh^2\left(\tilde{\kappa} \cos \frac{\tilde{\varphi}}{2}\right)} \quad (24)$$

with

$$\tilde{\varphi} = \arctan \frac{\omega}{\tilde{\omega}_c} \quad \text{and} \quad \tilde{\kappa} = \frac{l}{\tilde{\lambda}_p} \left(1 + \frac{\omega^2}{\tilde{\omega}_c^2} \right)^{1/4}$$

For $\varphi_l > 2b \ln(\lambda_p/\sqrt{2l})$ the spatial dependence of φ^0 cannot be neglected in Eq. (20). The solution of Eq. (20) leads to a hypergeometric equation which, due to the overall complexity, is not presented here. The outline of this solution is given in the Appendix. Numerical solutions of Eq. (20) are, however, obtained easily with standard mathematical software, e.g. using MAPLE. This numerical analysis is applicable under the prerequisite that \mathcal{C}_{dl} can still be considered independent of $\varphi^0(z)$ and, thereby, z -independent.

The type of impedance spectra as given by Eq. (24) is expected for the cathode catalyst layers of PEFC in the range of overpotentials defined by Eq. (23) with renormalized parameters prescribed by Eq. (21) and

$$\tilde{R}_{ct} = 2 R_{ct} \exp\left(-\frac{\varphi_l}{b}\right) \quad (25)$$

At $\omega = 0$ the real differential resistivity of the layer is obtained in terms of the renormalized parameters,

$$R_{diff} = \sqrt{R_p \tilde{R}_{ct}} \coth\left(\frac{l}{\tilde{\lambda}_p}\right) \quad (26)$$

4.2.3. Limiting frequency-regimes.

(a) For $\omega \gg \tilde{\omega}_c$, the complex impedance has a linear branch at an angle of 45° in the Cole–Cole representation, which is prescribed by

$$Z = \sqrt{\frac{R_p}{C_{dl}}} \omega^{-1/2} \frac{\sqrt{2}}{2} (1 - i) \quad (27)$$

Here, the impedance is independent of the working point, φ_b , and the frequency dependence is determined solely by the parameters of the composite, R_p and C_{dl} . For $l \ll \tilde{\lambda}_p$, the linear branch appears only at very high frequencies,

$$\omega \gg \omega_s \quad (28)$$

using a definition

$$\omega_s = \left(\frac{\tilde{\lambda}_p}{l}\right)^2 \tilde{\omega}_c = \left(\frac{\lambda_p}{l}\right)^2 \omega_c = \frac{\sigma}{\mathcal{C}_{dl}} \quad (29)$$

If for instance R_p is known from independent experimental data, the high frequency part of the impedance spectra will give C_{dl} . In this limit the proton transport and double layer charging effects determine the overall performance of the layer.

(b) For $\omega \ll \tilde{\omega}_c$, a Taylor-expansion in Eq. (24) gives

$$Z = R_{diff} \left(1 - A \left(\frac{l}{\tilde{\lambda}_p} \right) \left(\frac{\omega}{\tilde{\omega}_c} \right)^2 - i \frac{\omega}{\tilde{\omega}_c} B \left(\frac{l}{\tilde{\lambda}_p} \right) \right) \quad (30)$$

with functions

$$A(\xi) = \frac{1}{2} \left\{ 3 + 2\xi \frac{\frac{3}{2} + \xi \coth(\xi)}{\sinh(2\xi)} \right\}$$

$$B(\xi) = \frac{1}{2} \left\{ 1 + \frac{2\xi}{\sinh(2\xi)} \right\} \quad (31)$$

This asymptotic expansion forms a part of a semicircle in the complex plane of a Cole–Cole plot. This kind of behaviour indicates charge transfer limitations, bypassed through the double layer charging. The center of the semicircle is located on the real axis at

$$M = R_{diff} \left(1 - \frac{B^2}{2A} \right) \quad (32)$$

Its radius is given by

$$r = R_{diff} \frac{B^2}{2A} \quad (33)$$

4.3. Limiting thickness regimes

For $l/\tilde{\lambda}_p \rightarrow 0$, $M = r = R_{diff}/2$, the limitations due to proton transport are practically absent and the ac-

response in the Cole–Cole representation forms a perfect semicircle in the complex plane due to the parallel processes of charge transfer and double layer charging, whereas any oxygen or proton transport limitations can be neglected. The semicircular character of the impedance response is approximated better, the smaller the ratio $l/\tilde{\lambda}_p$. For a well-shaped semicircle, the frequency in the turning point equals the characteristic frequency $\tilde{\omega}_c$. The accuracy with which $\tilde{\omega}_c$ can be obtained by this simple graphical procedure depends on $l/\tilde{\lambda}_p$. If this ratio is small the method is highly accurate. For a ratio as large as $l/\tilde{\lambda}_p \lesssim 1$ the error of the estimation of $\tilde{\omega}_c$ lies within 10%.

The limiting case $\tilde{\kappa} \ll 1$ ($l \ll \tilde{\lambda}_p$, $\omega \lesssim \tilde{\omega}_c$) represents the dominance of charge transfer limitations due to the slow rate of Faradaic processes. Proton transport proceeds with a high rate and, therefore, the reaction acts are distributed homogeneously across the layer. The appearance of the semicircle is due to the parallel circuit of \tilde{R}_{ct} and C_{dl} . This semicircle is closer to perfect, the less severe are the proton transport limitations, i.e. the smaller is $l/\tilde{\lambda}_p$.

The linear response to a small signal in the Tafel-regime is characterized by the renormalized values $\tilde{\lambda}_p$, $\tilde{\omega}_c$, and \tilde{R}_{ct} . Close to the lower boundary of the potential range, Eq. (23), the penetration depth $\tilde{\lambda}_p$ will be large compared to the electrode thickness. With the increase of the electrode potential, however, the reaction penetration depth decreases exponentially, and the characteristic frequency increases exponentially. Once $\tilde{\lambda}_p$ approaches l , the differential electrode resistivity takes the form

$$R_{\text{diff}} \approx \sqrt{2R_p R_{ct}} \exp\left(-\frac{\varphi_l}{2b}\right) \quad (34)$$

i.e. the Tafel slope doubles. This effect is due to the ohmic losses of proton transport which become of equal importance as kinetic losses in the considered regime.

Thus, the graphical representation of impedance spectra provides definite tools for a determination of the catalyst layer parameters via the identification of the linear part and the branches of semicircular character.

5. Effect of O₂-transport

In the case when O₂-transport limitations cannot be neglected, the performance of the catalyst layer is prescribed by the full set of equations, Eqs. (1)–(3).

In the following subsections two approximations will be studied in order to calculate the effect of O₂-transport limitations on the complex impedance response of the layer. As a start, we consider the one in which only oxygen diffusion limitations are considered, whereas proton transport limitations are neglected. In the second approximation, both transport limitations are taken into account in the dynamic equations, but they are considered

to be still small enough to ignore the spatial dependences in the stationary parts. The most accurate solution which does not use these approximations can be obtained only numerically; it utilizes the first order expressions for the spatial variations of the stationary parts of the local overpotential, $\varphi^0(z)$, as well as the local oxygen partial pressure, $p^0(z)$.

5.1. Stationary solution

First, let us study the stationary solution for the case of negligible proton transport limitations. Here, the performance of the equipotential layer is determined solely by Eqs. (2) and (3). The combination of these equations leads to

$$\frac{d^2 p(z)}{dz^2} - \gamma^2 p(z) = 0 \quad \gamma = \sqrt{\frac{i_p}{I}} \equiv \exp(\varphi_0/2b) \sqrt{\frac{i^*}{I}} \quad (35)$$

The boundary conditions are

$$p(z=1) = 0 \quad \text{and} \quad \left. \frac{dp}{dz} \right|_{z=0} = 0$$

The solution of this equation is given by

$$p(z) = \frac{\cosh(\gamma z)}{\cosh(\gamma)} \quad (36)$$

Hence, using $j(z=1) = 0$ and Eq. (3)

$$j(z) = j_0 - I\gamma \frac{\sinh(\gamma z)}{\cosh(\gamma)} \quad (37)$$

The parametric form of the current-voltage plots is determined by

$$j_0 = I\gamma \tanh(\gamma) \\ \eta_0 = 2b \ln(\gamma) - b \ln\left(\frac{i^*}{I}\right) \quad (38)$$

This solution reveals two important effects:

- Since γ does not depend on p_0 and I , $i^* \propto p_0$ it follows that

$$j_0 \propto p_0$$

Hence, at a given electrode potential, the current density is proportional to the oxygen partial pressure at $z=1$.

- Since $I\gamma$ is independent of l and $\gamma \propto l$ ($\gamma = l/\delta_{\text{eff}}$),

$$j_0 \propto \tanh\left(\frac{l}{\delta_{\text{eff}}}\right),$$

with a diffusion-limited penetration depth

$$\frac{\delta_{\text{eff}}}{l} = \sqrt{\frac{I}{i^*}} \exp(-\varphi_0/2b).$$

Thus increasing the electrode thickness beyond 2–3 δ_{eff} will give only small improvements in performance.

In the case $l \ll \delta_{\text{eff}}$ the overall performance is determined simply by the reaction kinetics, $j_0 \approx i^* \exp(\varphi_0/b)$, whereas in the case $l \gg \delta_{\text{eff}}$ the performance has a double Tafel-law dependence on electrode potential, $j_0 \approx \sqrt{i^* I} \exp(\varphi_0/2b)$. The differential resistivity of the layer is given by

$$\mathcal{R}_{\text{diff}} = \frac{2b}{I} \frac{\cosh^2(\gamma)}{\gamma \sinh(\gamma) \cosh(\gamma) + \gamma^2} \quad (39)$$

5.2. Dynamic response

Let us now discuss formally the different ranges of parameters, where the expressions can be simplified significantly. In the discussion section we shall consider the physical conditions, when these ranges are realized.

5.2.1. Basic equations

The response to a small harmonic signal in a specified working point can be described by the same procedure as before, by using Fourier-transforms and splitting the physical variables into stationary and dynamic parts, according to Eq. (17) and

$$p(z, w) = p^0(z) + \delta p(z, w) \quad (40)$$

and subtraction of the stationary parts. Finally, the equations which determine the dynamic response are given by

$$\frac{d(\delta\varphi)}{dz} = -\frac{1}{\sigma} \delta j \quad (41)$$

$$\frac{d(\delta j)}{dz} = -i_p(z) \delta p - i_p(z) p^0(z) \frac{\delta\varphi}{b} - i\omega \mathcal{C}_{\text{dl}}(\delta\varphi) \quad (42)$$

$$\frac{d(\delta p)}{dz} = \frac{\delta j_0 - \delta j}{I} \quad (43)$$

to linear order in the perturbations. Terms which are of second or higher order in the dynamic variables are neglected. Here,

$$i_p(z) = i^* \exp\left(\frac{\varphi^0(z)}{b}\right)$$

its z -dependence coming from the finite proton conductivity.

In the high-frequency limit, $\omega \rightarrow \infty$, Eq. (43) decouples from Eqs. (41) and (42) which take on the form

$$\frac{d(\delta\varphi)}{dz} = -\frac{1}{\sigma} \delta j, \quad \frac{d(\delta j)}{dz} = -i\omega \mathcal{C}_{\text{dl}}(\delta\varphi) \quad (44)$$

Therefore, in this limit the performance is determined solely by proton transport limitations and the straight line branch of the complex impedance, given by Eq. (27), is retained.

5.2.2. Analytical solutions of dynamic equations.

5.2.2.1. *Fast proton transport, $\sigma = \infty$.* In this case $\varphi^0(z) = \varphi_0 = \varphi_r$. Variations in $\delta\varphi$ are negligible. The stationary solution for p^0 is used in Eq. (42). Differentiation of Eq. (42) and insertion of Eq. (43) gives

$$\frac{d^2 \mathcal{F}}{dz^2} - \gamma^2 \mathcal{F} = \gamma \mathcal{A} \sinh(\gamma z) \quad \text{with } \mathcal{F} = \delta j_0 - \delta j,$$

$$\mathcal{A} = \frac{i_p}{b \cosh(\gamma)} \delta\varphi \quad (45)$$

With the appropriate boundary conditions

$$J = 0 \text{ at } z = 0, \quad \delta p = 0 \text{ at } z = 1$$

the solution is given by equation

$$\delta j_0 = \frac{\mathcal{A}}{2} \left\{ \frac{\sinh(\gamma)}{\gamma} - \tanh(\gamma) \sinh(\gamma) + \cosh(\gamma) \right\} + i \frac{\mathcal{B}}{\gamma} \tanh(\gamma), \quad \mathcal{B} = \omega \mathcal{C}_{\text{dl}} \delta\varphi \quad (46)$$

The complex impedance then reads,

$$Z(\gamma, p_0, \eta_0) = \frac{R_r}{f_1(\gamma)} \frac{1 - i \frac{\omega f_2(\gamma)}{\omega_r f_1(\gamma)}}{1 + \left(\frac{\omega f_2(\gamma)}{\omega_r f_1(\gamma)} \right)^2} \quad (47)$$

where

$$R_r \equiv \frac{2b}{i_p}, \quad \omega_r \equiv \frac{1}{R_r \mathcal{C}_{\text{dl}}}$$

$$f_1(\gamma) \equiv \frac{\tanh(\gamma)}{\gamma} + \frac{1}{\cosh^2(\gamma)}, \quad f_2(\gamma) \equiv \frac{\tanh(\gamma)}{\gamma}$$

The differential resistivity, obtained from this equation for $\omega = 0$, is given by the same expression as in Eq. (39). The linear response prescribes a perfect semicircle in the complex plane without a linear branch.

5.2.2.2. *Negligible spatial dependencies in the stationary parts of overpotential, φ^0 , and O_2 -partial-pressure, p^0 .* Taking into account such dependencies in the respective dynamic parts, the following equation is obtained as the simplest extension of Eq. (45) with due account of oxygen transport limitations:

$$\frac{d^2(\delta j)}{dz^2} - \frac{l^2}{\lambda^2} \delta j = -\gamma^2 \delta j_0 \quad (48)$$

with

$$\lambda = \left(\gamma^2 + \frac{l^2}{\lambda_p^2} \left(1 + i \frac{\omega}{\omega_c} \right) \right)^{-1/2} = \frac{\lambda_p}{l \sqrt{1 + g^{-1}}} \left(1 + i \frac{\omega}{\omega_{c2}} \right)^{-1/2}$$

where

$$\omega_{c2} = \tilde{\omega}_c(1 + g^{-1})$$

The solution of this equation with the boundary conditions

$$\delta j = \delta j_0 \text{ at } z = 0,$$

$$\delta p = 0 \text{ at } z = 1 \text{ and } \delta j = 0 \text{ at } z = 1$$

reads

$$\delta j(z, w) = j_0 \left\{ \lambda^2 \gamma^2 + (1 - \lambda^2 \gamma^2) \cosh\left(\frac{z}{\lambda}\right) - \left[(1 - \lambda^2 \gamma^2) \coth\left(\frac{1}{\lambda}\right) + \frac{\lambda^2 \gamma^2}{\sinh\left(\frac{1}{\lambda}\right)} \right] \sinh\left(\frac{z}{\lambda}\right) \right\} \quad (49)$$

This solution can be used in Eqs. (41) and (43). Subsequent integrations will give expressions for δp and $\delta \varphi$. The complex impedance takes on the form

$$Z = \frac{\delta \varphi_0}{\delta j_0} = \frac{1}{\sigma} \left\{ \frac{\lambda_p^2}{I^2} \frac{1 - \lambda^2 \gamma^2 + \lambda^2 \gamma^2 \cosh\left(\frac{1}{\lambda}\right)}{\left(1 + i \frac{\omega}{\tilde{\omega}_c}\right) \lambda \sinh\left(\frac{1}{\lambda}\right)} + \lambda^2 \gamma^2 + \lambda \frac{\cosh\left(\frac{1}{\lambda}\right) - 1}{\sinh\left(\frac{1}{\lambda}\right)} \right\} \quad (50)$$

This expression gives the limiting behaviour in the zero frequency limit ($\omega \rightarrow 0$) for $I \gg \sigma b$

$$R_{\text{diff}} \approx \sqrt{\frac{b}{\sigma i_p}} \coth\left(\sqrt{\frac{i_p}{\sigma b}}\right) \quad (51)$$

and for $(i_p \ll) I \ll \sigma b$

$$R_{\text{diff}} \approx \frac{b}{\sqrt{I i_p}} \coth\left(\sqrt{\frac{i_p}{I}}\right) \quad (52)$$

In the high-frequency limit the impedance is given by Eq. (27). In the zero-frequency limit the differential resistivity is, thus, obtained in the same form in the limiting cases of either dominating proton- or O_2 -transport-limitations. The difference between the expressions Eqs. (51) and (52) is accounted for by the replacement of σb by I . In the high-frequency limit the response is prescribed by Eq. (27) which is determined by proton transport limitations. The approximation presented here, gives, however, good results only in an intermediate regime, in which neither proton transport nor oxygen diffusion are the limiting processes, i.e. for $\tilde{\lambda}_p, \delta_{\text{eff}} \gtrsim 2l$.

5.2.2.3. Improved approximate solution. This can be obtained from the complete set of equations, Eqs. (41)–(43), if the stationary solutions of $\varphi^0(z)$ from Eq. (12) and of $p^0(z)$ from Eq. (36) are used in Eq. (42)³. This solution will apply in parameter-regimes in which $\tilde{\lambda}_p, \delta_{\text{eff}} \lesssim 1$.

One of the three dynamic variables can be removed by combination and subsequent integration of Eqs. (41) and (43), which leads to a relation between $\delta \varphi(z)$ and $\delta p(z)$,

$$\delta p(z) = \frac{\sigma b}{I} (\delta \varphi - \delta \varphi_i) + \frac{\delta j_0}{I} (z - 1) \quad (53)$$

This can be inserted into Eq. (42). After splitting the variables into real and imaginary parts,

$$\delta \varphi = \delta \varphi^{(1)} + i \delta \varphi^{(2)}, \quad \delta j = \delta j^{(1)} + i \delta j^{(2)}$$

the resulting system of differential equations reads

$$\frac{d(\delta \varphi^{(1)}(z))}{dz} = -\frac{1}{\sigma} (\delta j^{(1)}(z)) \quad (54)$$

$$\frac{d(\delta \varphi^{(2)}(z))}{dz} = -\frac{1}{\sigma} (\delta j^{(2)}(z)) \quad (55)$$

$$\frac{d(\delta j^{(1)}(z))}{dz} = -\frac{i^* \exp\left(\frac{\varphi_i^0}{b}\right)}{\cos^2(\zeta(1-z))} \times \left\{ \left[\frac{\sigma b}{I} + \frac{\cosh(\gamma z)}{\cosh(\gamma)} \right] \frac{\delta \varphi^{(1)}(z)}{b} + \frac{\delta j_0^{(1)}}{I} (z - 1) - \frac{\sigma b}{I} \frac{\delta \varphi_i^{(2)}}{b} \right\} + \omega \mathcal{E}_{\text{ai}} \delta \varphi^{(2)}(z) \quad (56)$$

$$\frac{d(\delta j^{(2)}(z))}{dz} = -\frac{i^* \exp\left(\frac{\varphi_i^0}{b}\right)}{\cos^2(\zeta(1-z))} \times \left\{ \left[\frac{\sigma b}{I} + \frac{\cosh(\gamma z)}{\cosh(\gamma)} \right] \frac{\delta \varphi^{(2)}(z)}{b} + \frac{\delta j_0^{(2)}}{I} (z - 1) - \frac{\sigma b}{I} \frac{\delta \varphi_i^{(2)}}{b} \right\} - \omega \mathcal{E}_{\text{ai}} \delta \varphi^{(1)}(z) \quad (57)$$

$\delta j_0^{(1)}$ and $\delta j_0^{(2)}$ are to be determined self-consistently by an iterative procedure, using

$$\delta j^{(1)}(z=0) = \delta j_0^{(1)} \text{ and } \delta j^{(2)}(z=0) = \delta j_0^{(2)}$$

³ These stationary solutions have been obtained in the complementary limiting cases, when one of the two transport processes dominates, whereas the other one is negligible. Mutually correlated effects on the performance between the stationary pressure profile (Eq. (36)), and the distribution of electrode potential (Eq. (12)), i.e. the effect of $p^0(z)$ -profile on $\varphi^0(z)$ -profile and vice versa, are not taken into account.

Differences between the analytical solutions and the more accurate numerical solution are small if the reaction penetration depth due to proton transport limitations is large compared to the electrode thickness. In particular for compositions with large amounts of electrolyte within the layer, when diffusion limitations are of high significance, the approximate expression Eq. (47) works sufficiently well.

6. Parameterization of the composition-dependence

The working point of the electrode (j_0) is specified by fixing the value of φ_l . The thickness dependence is contained explicitly in the definitions of elementary parameters, σ , I , i^* and C_{dl} . In addition these parameters are also composition-dependent. Parameterizations of these composition-dependences are the subject of this section. Formulae which determine explicitly the dependence of the elementary parameters on the electrolyte content x in the layer have been proposed in Ref. [10]. Similar parameterizations, summarized in Fig. 2, are used here. They will help us in the end to understand the composition dependence of the complex impedance.

For the conductivity, the expression

$$\sigma(x) = \sigma_s \frac{(x - x_c)^\tau}{(1 - x_c)^\tau} \Theta(x - x_c) \quad (58)$$

is used. Θ is the Heaviside-step-function. The critical exponent τ is universal, i.e. independent of the structure of the composite, but it depends on the system dimensionality. In three dimensions $\tau \approx 2$ [19,20]. The percolation-threshold x_c depends on the geometry of the lattice. If the pore space is highly coordinated as in a densely packed structure where a single pore has 12 nearest neighbor pores, x_c is small (≈ 0.19 for the site-percolation and ≈ 0.12 for the bond-percolation

problem [20]). Poorly connected pore spaces, such as a diamond lattice, can have percolation thresholds as large as 0.4. We will assume, here, values in the range $x_c \sim 0.1$ to 0.2. $\sigma_s = \sigma(x = 1)$ stands for the conductivity of the layer, if its macropore system is fully saturated with electrolyte⁴.

The major pathways for O_2 -diffusion go through the voids which are free from electrolyte. We approximate the x -dependence of the parameter introduced in Eq. (3) by

$$I(x) = I_s \frac{\Theta(1 - x - x_c)(1 - x - x_c)^\tau + d\{1 + (1 - x)^\tau \exp(1 - (1 - x - x_c)/2)\}}{(1 - x_c)^\tau + d\{1 + \exp(-(1 - x_c)/2)\}} \quad (59)$$

which again rests on the percolation-type dependences [19–21]. Here, the coefficient d accounts for the residual diffusivity due to diffusion through micropores or polymer material as these pathways are free, if even all macropores are ‘blocked’ by electrolyte. Typically, their contribution to I is small, and, thus, $d \ll 1$. I_s is the diffusivity of the open system, not containing any PFSI.

The parameter for the exchange current density is proportional to the specific area of the Pt|PFSI interface which is accessible for protons as well as for O_2 ,

$$i^*(x) = i_s^* x \mathcal{P}(x) \{1 - [1 - (1 - x)\mathcal{P}(1 - x)]^\mathcal{Z}\} \quad (60)$$

Here, i_s^* is the exchange current density for the case if all the Pt-particles on the outer agglomerate surfaces are covered by electrolyte and if all of these sites can be reached by protons as well as by O_2 . \mathcal{Z} is the coordination number of a single site, i.e. the number of bonds to other sites. With a PFSI portion proportional to x , only the fraction x of all Pt places is covered by electrolyte. This is reflected by the factor x on the rhs of Eq. (60). The product of the last two factors ensures that the Pt|PFSI-contacts are connected simultaneously to the sample spanning networks of electrolyte $\mathcal{P}(x)$, as well as to that of the gas pores (through macropores), the last factor in curly brackets. The conditional probability \mathcal{P} is parameterized by the function⁵

$$\mathcal{P}(x) = \exp(-(x - x_m)) \left(\frac{x - x_c}{x_m - x_c} \right) \Theta(x_m - x) \Theta(x - x_c) + \Theta(x - x_m) \quad (61)$$

⁴ Surprisingly, the scaling law Eq. (58) works not only near the percolation threshold, but approximates fairly well the whole $\sigma(x)$ -dependence [21].

⁵ \mathcal{P} denotes the probability with which an occupied lattice site belongs to the infinite cluster of occupied lattice sites.

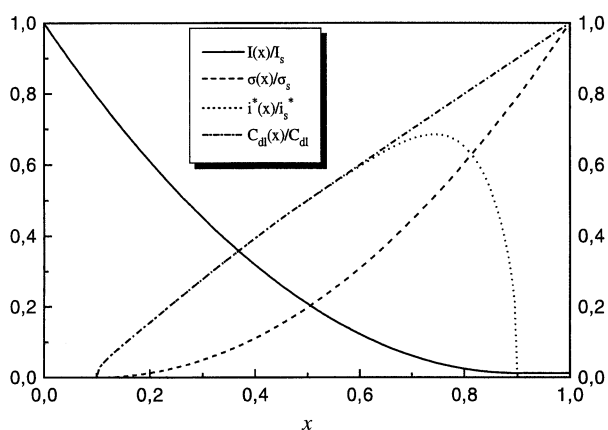


Fig. 2. Composition-dependent parameters of the catalyst layer, parameterized as a function of the electrolyte content x .

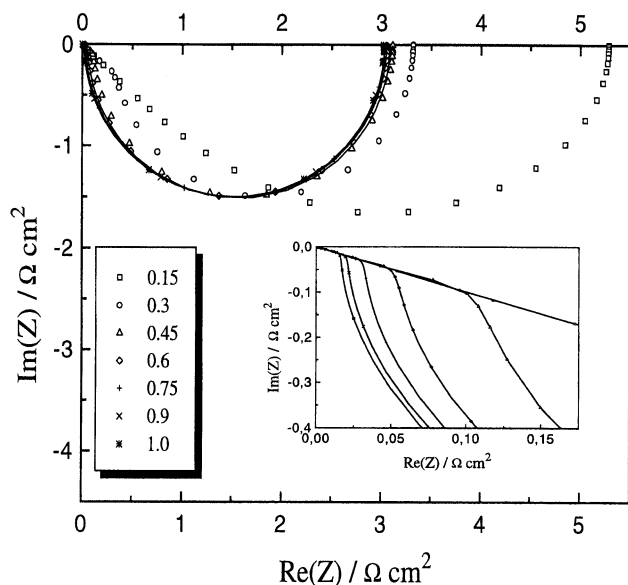


Fig. 3. Composition dependent impedance spectra at $j_0 = 0.01 \text{ A cm}^{-2}$. The spectra are calculated analytically from Eq. (24) (lines) or numerically from Eq. (20) (dots). The reference parameters used are $b = 0.03 \text{ V}$, $i^* = 3 \times 10^{-5} \text{ A cm}^{-2}$, $\sigma = 20 \text{ Ω cm}^{-2}$, $l = 10 \text{ μm}$. The composition dependence is controlled by varying the fraction of electrolyte. It is parameterized according to equations of percolation theory, Eqs. (58)–(60) and (62), which were discussed in Ref. [10]. A good correspondence between the numerical and analytical results is obtained only at large x , i.e. for good proton conductivity.

At $x \geq x_m$, $\mathcal{P} = 1$. Specific values of the parameter x_m as well of x_c depend on the lattice-type on which the model of void spaces is mapped. Critical exponents s can be taken from experimental/theoretical studies on percolation properties of random, composite media. These studies suggest using $s = 0.4$. x_m is a parameter fitted in order to obtain a smooth approach of \mathcal{P} to 1.

The double layer capacitance of the layer, \mathcal{C}_{dl} , is determined by the specific contact area S_{dl} between metal parts (carbon, Pt) and electrolyte fractions of the connected PFSI-cluster. An expression for the composition dependence of \mathcal{C}_{dl} can be written in the following form,

$$\mathcal{C}_{dl} = \mathcal{C}_{dl}^s x^{\mathcal{P}(x)} \quad (62)$$

where \mathcal{C}_{dl}^s is the double layer capacitance of a system that is completely filled with electrolyte. Note that the accessibility to the gas pore-network is not a prerequisite for a piece of the contact area in order to contribute to the double layer charging.

7. Electroanalysis of the catalyst layer by means of impedance spectra

As we have shown, the character of impedance spectra is influenced by the variation of the key properties

and operating conditions of the layer. In this section impedance spectra will be discussed from a physical point of view. The expressions derived will be used to investigate the effects of composition, thickness and working point specification.

7.1. The high-frequency limit

The behaviour of the electrode in the high-frequency limit is independent of any of the approximations. The frequency dependence in this part of the spectra is predicted correctly by Eq. (27). In the Cole–Cole representation the response in this regime prescribes a straight line at a 45°-angle, see for instance Fig. 3 or Fig. 4. Double layer charging effects and proton transport dominate the overall electrode response in this regime. An equivalent circuit which reproduces this small signal response is represented by an RC-transmission line, c.f. Fig. 1. Faradaic processes are not significant due to the high frequencies. Since no branching or fractality of the network is assumed, this response resembles that of a Warburg impedance [22] with a characteristic proportionality

$$|Z| \propto \omega^{-1/2}$$

The proportionality constant $\sqrt{R_p/C_{dl}}$ is a characteristic function of the composition.

A frequency-dependent penetration depth may be defined by

$$\lambda_\omega = \sqrt{\frac{\sigma}{\omega \mathcal{C}_{dl}}} l \quad (63)$$

which becomes very small at large ω . The plot of $|Z|$ versus $\omega^{-1/2}$ will give $\sqrt{R_p/C_{dl}}$ as its slope. This slope may be used in order to study composition-dependent effects. If, for instance, the composition dependence of R_p is known from independent ex-situ conductivity measurements or from theoretical considerations based

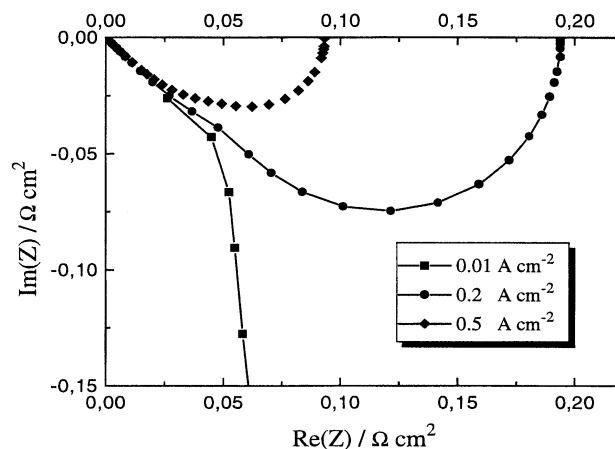


Fig. 4. Effect of the working point (different values of j_0 , as specified in the legend) on the impedance spectra for $x = 0.6$ and $l = 10 \text{ μm}$.

on concepts of percolation theory, then the composition dependence of C_{dl} may be inferred from this kind of plot.

From the composition dependence of R_p , which is determined by the volume fraction and connectivity of electrolyte in the layer, and of C_{dl} , which is determined by the contact area between metal (carbon, Pt) and electrolyte, important conclusions may be drawn about the electrolyte distribution in the catalyst layer and its effect on the performance.

The relevant frequency domain in which the measurements have to be performed in order to reveal these effects is determined by Eq. (28). The lower boundary on the frequency is independent of the working point. An order of magnitude estimate with $\sigma = 20 \text{ S cm}^{-2}$ and $C_{dl} = 100 \text{ F cm}^{-2}$ gives a value of $\omega_s \sim 10^5$ to 10^6 s^{-1} for this characteristic frequency.

7.2. Characteristic length-scales

The interplay between the two distinct, complementary transport limitations and losses due to reaction kinetics can be rationalized by means of two distinct length scales. These are the potential-dependent characteristic reaction penetration depth, $\tilde{\lambda}_p$, which is due to proton transport limitations and the characteristic length of oxygen diffusion, δ_{eff} .

Let O_2 -transport limitations be negligible ($\delta_{eff} \gg l$) and only proton transport limitations significant, though still relatively small ($\tilde{\lambda}_p \gtrsim 2l$). Here, the approximation given by Eq. (24) gives good results. However, since the impedance response in this regime is determined mainly by charge transfer and double layer charging, the overall effect of proton conductivity, observable in the spectra, is small. Within this approximation impedance spectroscopy bears a diagnostic message only at high ω , in the linear part of the spectra, since it reveals the interplay between proton conductivity and double layer capacitance (according to Eq. (27)). If O_2 -transport limitations are still negligible, but proton transport limitations are strong ($\tilde{\lambda}_p \lesssim 2$), then numerical solutions of Eq. (20) have to be used for the electrode characterization.

The opposite case arises if proton transport is excellent ($\tilde{\lambda}_p \gg l$), but oxygen supply is the limiting process ($\delta_{eff} \lesssim l$). Here, the performance is determined by Eq. (47).

The different limiting cases as well as the intermediate cases, for which numerical solutions can be obtained, can be realized by controlling the composition of the layer. Useful diagnostic tools emerging from this option will be discussed in the following subsections.

7.3. Effect of proton conductivity

Typical sets of impedance spectra in the case of negligible oxygen transport limitations are depicted in

Table 1

Calculated parameters which characterize the catalyst layer performance in the limit of vanishing oxygen diffusivity for various compositions at $j_0 = 0.01 \text{ A cm}^{-2}$ ^a

x	φ_l/V	φ_0/V	$\tilde{\lambda}_p/l$	λ_p^*/l	ω_c^*
0.15	0.225	0.248	18.3	0.60	902
0.30	0.211	0.214	42.0	1.77	568
0.45	0.198	0.199	58.1	3.04	365
0.60	0.189	0.190	72.0	4.33	277
0.75	0.183	0.183	83.4	5.61	221
0.90	0.177	0.177	93.7	6.90	185
1.00	0.174	0.174	100.0	7.76	166

^a Reference parameters are specified in the caption of Fig. 2

Fig. 3 for a specified reference parameter set at a current density $j_0 = 0.01 \text{ A cm}^{-2}$. Variations of the composition are controlled by means of x (legend). Calculated parameters of the layer which correspond to the different x are shown in Table 1. The solid lines are calculated within the approximation of Eq. (24), whereas the symbols represent the numerical solutions of Eq. (20). Evidently, where the approximate solution, Eq. (24), works well, lines and symbols coincide. At very high frequencies, for which the crossover from the semicircular behaviour to the straight line part occurs, the approximation leads to good results for all compositions (as shown in the insert of Fig. 3).

Considerable effects of the electrolyte fraction on the differential resistivity are expected only for x close to x_c , when the electrolyte conductivity becomes rather poor. In this way, the impedance spectra provide a means for the structural characterization of the layer. The spectra show how, with decreasing electrolyte content and, thus, increasing cathodic overpotential the real resistivity increases and the linear high frequency branch becomes more important, since the reaction penetration depth decreases⁶.

Fig. 4 shows the effect of different working conditions, i.e. different values of j_0 for fixed composition ($x = 0.6$) and thickness ($l = 10 \text{ }\mu\text{m}$). R_{diff} is smaller for higher j_0 . At large j_0 proton transport limitations become more severe in comparison to the reaction kinetics. The straight line is, therefore, more significant. For a fixed electrode composition $x = 0.6$, the effect of the electrode thickness l on the complex impedance is depicted in Fig. 5. Larger l causes an increase in R_{diff} .

⁶ If $\tilde{\lambda}_p$ is, however, small, the approximation of a constant overpotential in the cathode layer becomes worse. This is indicated by the comparison of the approximate analytical solution with the accurate numerical solution. For a given cathodic overpotential-bias $\varphi^0(z)$ the approximation of a constant value for it, used in Eq. (24), will overestimate the decrease of the reaction penetration depth.

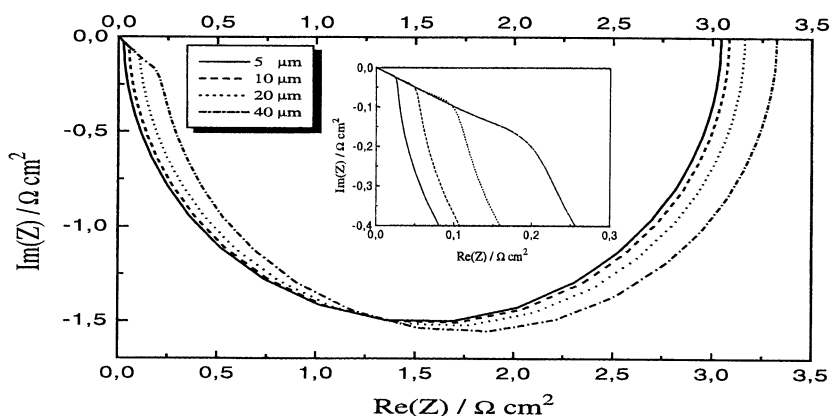


Fig. 5. Effect of variation of layer-thickness l on impedance spectra for $x = 0.6$ and $j_0 = 0.01 \text{ A cm}^{-2}$.

7.4. Effect of O_2 -transport

The opposite limit to the two cases discussed in the previous subsection arises when proton transport is fast ($\tilde{\lambda}_p \gg l$), but oxygen transport limitations are considerable ($\delta_{\text{eff}} \lesssim 2l$). This situation may be realized for large values of x , for which a sufficient gas porosity cannot be provided. Effects in impedance spectra which are caused by oxygen diffusion limitations are depicted in Fig. 6. These spectra are calculated using Eq. (47).

In Fig. 7 the variation of the differential resistivity, c.f. Eq. (39), is shown as a function of x for different values of the diffusion parameters I_s and d and for different working points. A considerable effect due to oxygen diffusion will appear in the spectra only for large x close to $1 - x_c$, when the diffusivity becomes small. This effect can, thus, be used for the characterization of the percolation properties of the layer with respect to oxygen diffusion.

Another case which can be treated by analytical expressions is realized, when both proton- and oxygen-transport limitations are remarkable, but not really strong ($\tilde{\lambda}_p, \delta_{\text{eff}} \approx 2l$). Impedance spectra are then calculated using Eq. (50). In this case the linear high frequency branch shows up again, indicative of considerable proton transport limitations. This type of spectrum is plotted in Fig. 6.

These analytical results may, of course, be misleading if they are plotted in parameter ranges where the prerequisites of their validity are not fulfilled. Obviously the approximation of Eq. (50) gives good results only when the oxygen diffusivity is not too bad. When it is poor, ‘qualitatively new features’ appear in the calculated spectra such as two separate semicircles. They are, however, artifacts. This becomes evident in Fig. 6 by the comparison with the more complete numerical solution of Eqs. (54)–(57).

8. Comparison with experiment

Experimental studies which relate effects of Nafion[®] impregnation to the performance of PEFC-electrodes have been presented by Lee et al. in [23]. These data are reproduced in Fig. 8. They demonstrate the qualitative correctness of the theoretical results obtained here. These authors found an optimum Nafion[®]-loading (solubilized Nafion[®] 1100) of 1.9 mg cm^{-2} in the H_2/O_2 -PEFC-mode. The data clearly reflect the competition between the three major functions of the catalyst layer (proton transport, oxygen supply, electrochemically active surface area), c.f. also Ref. [10].

The potential dependence of impedance spectra was studied by Paganin et al. in Ref. [24]. Potential dependent features are attributed to electrode processes. The effects observed in the Cole–Cole plots, presented there, closely resemble the theoretical findings described in this article.

In order to compare theoretical results and experimental data, the composition and composition dependent parameters, the thickness of the active layer and the working point (j_0, φ_0) have to be monitored simultaneously. A deficiency of the model presented here is that it does not properly include processes at the membrane|catalyst layer interface. These interfacial phenomena may, however, become dominant at low Nafion[®]-loadings, i.e. below 0.6 mg cm^{-2} (according to [23]), when the interior volume of the layer is practically inactive.

9. Conclusions

According to this study the main diagnostic features and recipes for the characterization of catalyst layers are as follows:

(a) If the characteristic length scales of both transport processes (O_2 and H^+) are large compared to

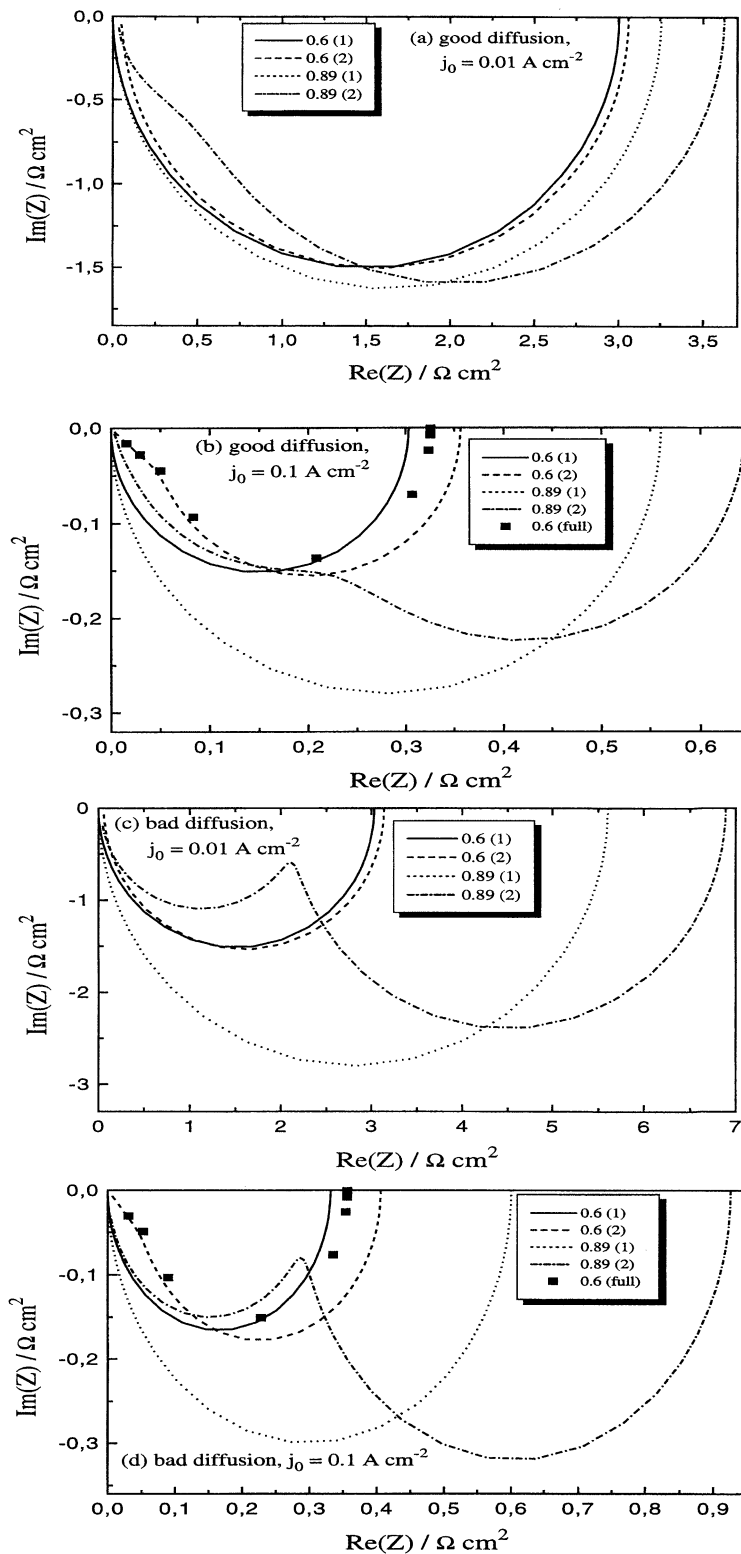


Fig. 6. Effect of finite oxygen diffusivity on impedance spectra for different compositions ($x = 0.6, 0.89$). Spectra are calculated within the different approximations, given by (1) Eq. (47) or (2) Eq. (50). For different working point specifications ($j_0 = 0.01, 0.1 \text{ A cm}^{-2}$) cases of good ($I_s = 30 \text{ A cm}^{-2}, d = 0.001$) and poor ($I_s = 3 \text{ A cm}^{-2}, d = 0.001$) oxygen diffusivity are compared. For poor oxygen diffusivity (x close to $1 - x_c$ or j_0 large) the approximate solution given by Eq. (50) gives qualitatively wrong results (the two resolved semicircles) and the full solution of the set of Eqs. (54) and (55) has to be used (points).

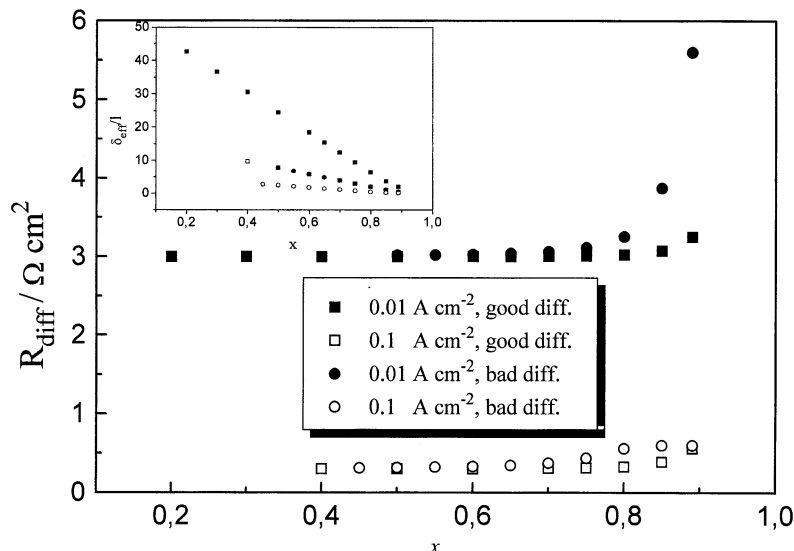


Fig. 7. Effect of oxygen diffusivity on the differential resistivity R_{diff} and on the characteristic length δ_{eff} (limited oxygen diffusivity) as a function of x . The effect is considerable only close to the percolation threshold.

the catalyst layer thickness, then the impedance response consists merely of a semicircle in the Cole-Cole representation. The differential resistivity (twice the value of the radius of the semicircle) depends mostly on the charge transfer resistivity R_{ct} (i.e. on the exchange current density parameter i^* and on the Tafel-slope b) and on the working point specification, which is fixed through φ_r .

(b) An exclusive indication of proton transport limitations is the straight line feature in the spectra. It is more pronounced in the high frequency domain, the smaller is the proton conductivity relative to the renormalized charge transfer resistivity. The straight line signature can provide information about the localization and distribution of the catalyst and electrolyte in the layer. This impedance response corresponds to the equivalent circuit of a linear ladder network composed of the distributed proton resistivities and capacities.

(c) Strong effects of proton transport and oxygen diffusivity on the differential resistivity arise close to the respective percolation thresholds, when one of the two processes limits the overall conversion rate of the electrode. These effects can be used for the determination of the percolation thresholds of proton conductivity and oxygen diffusivity.

Appendix A

A.1. Exact analytical solution

The starting point is Eq. (20). The substitution of $y = \zeta(1 - z)$ leads to

$$\delta\varphi''_{yy} = \frac{1}{A^2} \left(\frac{1}{\cos^2 y} + i\Omega \right) \delta\varphi \quad (\text{A.1})$$

where $A = \zeta \tilde{\lambda}_p(\varphi_r)$, $\Omega = \omega / \tilde{\omega}_c(\eta_1)$, and ' denotes derivative with respect to y .

Substitution of $x = y/2 + \pi/4$ gives

$$\delta\varphi''_{xx} - \frac{1}{A^2} (\tan^2(x) + \cot^2(x) + 2 + 4i\Omega) \delta\varphi = 0 \quad (\text{A.2})$$

Now, a further substitution of $u = \sin^2(x)$ and $\delta\varphi = w \sin^n(x) \cos^m(x)$, where n and m are roots of

$$n^2 - n + \frac{1}{A^2} = 0 \quad \text{and} \quad m^2 - m + \frac{1}{A^2} = 0$$

is used. Here, the set

$$n = m = \frac{1}{2} + \sqrt{\frac{1}{4} + \frac{1}{A^2}}$$

is specified. The differential-equation now reads

$$4u(u-1)w''_{uu} + 2[(4+2\mathcal{L})u - (2+\mathcal{L})]w'_u + \left((1+\mathcal{L})^2 + \frac{4i\Omega}{A^2} \right) w = 0 \quad (\text{A.3})$$

Finally this equation can be transformed to the standard form of the hypergeometric differential equation

$$u(u-1)w''_{uu} + [(\alpha+\beta+1)u - \gamma]w'_u + \alpha\beta w = 0 \quad (\text{A.4})$$

by means of notations

$$\alpha + \beta + 1 = 2 + \mathcal{L}, \quad \alpha\beta = \frac{(1+\mathcal{L})^2}{4} + \frac{i\Omega}{A^2},$$

$$\gamma = \frac{2+\mathcal{L}}{2}$$

thus,

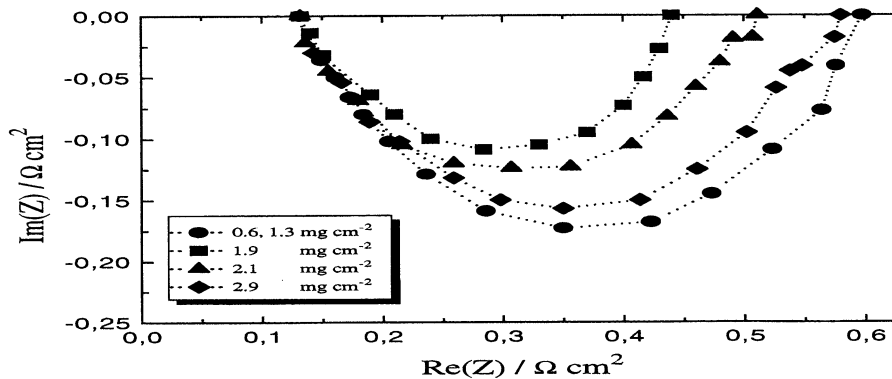


Fig. 8. Experimental data on complex impedance of cathode catalyst layers in PEFC (H_2/O_2) at varying fractions of embedded PFSI, extracted from Lee et al., fig. 5 in Ref. [23]. The constant high frequency limit of these impedance data is due to the membrane resistance.

$$\alpha = \frac{\mathcal{L} + 1}{2} \pm \sqrt{2 \left(\frac{\mathcal{L} + 1}{2} \right)^2 + \frac{i\Omega}{A^2}} \quad (\text{A5})$$

$$\beta = -\frac{\mathcal{L} + 1}{2} \pm \sqrt{2 \left(\frac{\mathcal{L} + 1}{2} \right)^2 + \frac{i\Omega}{A^2}} \quad (\text{A6})$$

The general solution of Eq. (A4) is given by

$$w(u) = \mathcal{A}w_1(u) + \mathcal{B}w_2(u) \quad (\text{A7})$$

with

$$w_1(u) = F(\alpha, \beta; \gamma; u) \quad (\text{A8})$$

$$w_2(u) = u^{1-\gamma} F(1-\gamma+\alpha, 1-\gamma+\beta; 2-\gamma; u) \quad (\text{A9})$$

where the hypergeometric function is defined by the series

$$F(\alpha, \beta, \gamma, u) = \sum_{k=0}^{\infty} \frac{(\alpha)_k (\beta)_k}{k! (\gamma)_k} u^k, \quad |u| < 1 \text{ (radius of convergence)} \quad (\text{A10})$$

and

$$(\lambda)_k = \lambda(\lambda+1)\dots(\lambda+k-1), \quad (\lambda)_0 = 1$$

First the working point has to be fixed by specifying φ_l . The boundary conditions at $z=1$ (a fixed, finite value of $\delta\varphi$ and $d(\delta\varphi)/dz=0$) must be used in order to determine the parameters \mathcal{A} and \mathcal{B} . Using the solution on $\delta\eta$ in Eq. (19) will give δj , and their ratio will give the complex impedance.

Appendix B

B.1. Nomenclature

Roman letters

- B apparent Tafel slope (V)
 c_{H^+} proton concentration (constant) (mol l^{-1})
 $c_{\text{O}_2}^*$ oxygen concentration at catalyst layer | backing layer interface (mol l^{-1})
 \mathcal{C}_{dl} parameter of double layer capacitance in continuum model (F cm^2)

- C_{dl} double layer capacitance-element in transmission line (F cm^2)
 D^0 effective diffusion constant of oxygen diffusion in the catalyst layer ($\text{cm}^2 \text{s}^{-1}$)
 D parameter of residual diffusivity, non-dimensional
 F Faraday constant, $F = 96487 \text{ A s mol}^{-1}$
 I characteristic parameter of oxygen diffusion, $I = 4F_p D^0 / RTl$ (A cm^{-2})
 I_s characteristic parameter of oxygen diffusion of a layer without any PFSI (A cm^{-2})
 i^* exchange current density parameter, $i^* = FS_0 k^* (c_{\text{H}^+})^\nu c_{\text{O}_2}^*$ (A cm^{-2})
 i_s^* exchange current density parameter if all Pt-particles in the layer would contribute to the active surface of electrochemical reaction (A cm^{-2})
 J Faradaic current density (A cm^{-2})
 $j(z)$ proton current density (A cm^{-2})
 j_0 proton current density entering the cathode at the catalyst layer | membrane interface (A cm^{-2})
 k^* rate constant of electrochemical reaction (cm s^{-1}) (mol l^{-1}) $^{-\nu}$
 L catalyst layer thickness (μm)
 \mathcal{P} conditional probability that a single Pt | PFSI-site belongs to the infinite cluster of PFSI, $\mathcal{P}(x)$, or gas pores, $\mathcal{P}(1-x)$
 $p(z)$ oxygen partial pressure, non-dimensional, normalized to P_0
 P_0 oxygen partial pressure at the gas backing side (atm)
 R universal gas constant, $R = 8.3143 \text{ J K}^{-1} \text{ mol}^{-1}$
 R_{ct} charge transfer resistance-element in transmission line equivalent circuit
 R_p protonic resistance-element in transmission line equivalent circuit
 S critical exponent in conditional probability \mathcal{P}
 S_0 effective surface of the Pt | PFSI contact area (cm^{-1})
 S_{dl} effective surface of the metal | PFSI contact area (cm^{-1})

T	temperature (K)
X	portion of PFSI-filled pores
x_c	critical portion of PFSI-filled pores (percolation threshold)
x_m	parameter in expression for \mathcal{P}
z	coordinate in the lateral direction across the catalyst layer, normalized to its thickness l , non-dimensional
\mathcal{Z}	coordination number of pores
<i>Greek letters</i>	
δ_{eff}	thickness of active part of the catalyst layer (due to O_2 depletion) (μm)
Θ	Heaviside-step function
λ	reaction penetration depth due to proton transport/ μm
ν	exponent in expression for i^*
σ_p	specific proton conductivity (S cm^{-1})
σ	proton conductivity, normalized to thickness, $\sigma = \sigma_p/l$ (S cm^{-2})
σ	proton conductivity of the layer if it is saturated with PFSI (S cm^{-2})
τ	critical exponent in percolation dependencies of conductivity and diffusivity
φ	local electrode potential, potential difference between electrolyte phase and electrode phase (equipotential) (V)
φ_0	catalyst layer electrode overpotential ($= \varphi(z = 0)$)
ω	frequency of harmonic signal (s^{-1})

References

- [1] M. Uchida, Y. Aoyama, X. Eda, A. Ohta, J. Electrochem. Soc. 142 (1995) 463.
- [2] M. Uchida, Y. Aoyama, N. Eda, A. Ohta, J. Electrochem. Soc. 142 (1995) 4143.
- [3] S. Escibano, P. Aldebert, Solid State Ionics 77 (1995) 318.
- [4] K. Bolwin, E. Güllow, D. Bevers, W. Schnurnberger, Solid State Ionics 77 (1995) 324.
- [5] S. Gottesfeld, T.A. Zawodzinski, in: R.C. Alkire, H. Gerischer, D.M. Kolb, C.N.V. Tobias (Eds.), Advances in Electrochemical Science and Engineering, vol. 5, Wiley-VCH, Weinheim, 1997, pp. 195–301.
- [6] M.S. Wilson, J.A. Valerio, S. Gottesfeld, Electrochim. Acta 40 (1995) 355.
- [7] M.S. Wilson, S. Gottesfeld, J. Appl. Electrochem. 22 (1992) 1.
- [8] M.S. Wilson, S. Gottesfeld, J. Electrochem. Soc. 139 (1992) L28.
- [9] S. Srinivasan, E.A. Ticianelli, C.R. Derouin, A. Redondo, J. Power Sources 22 (1988) 359.
- [10] M. Eikerling, A.A. Kornyshev, J. Electroanal. Chem. Soc. 453 (1998) 89.
- [11] T.E. Springer, I.D. Raistrick, J. Electrochem. Soc. 136 (1989) 1594.
- [12] I.D. Raistrick, Electrochim Acta 35 (1990) 1579.
- [13] K. Mund, F.V. Sturm, Electrochim. Acta 20 (1974) 463.
- [14] I. Rousar, K. Micka, A. Kimla, Electrochemical Engineering II, Part F, Elsevier, Amsterdam, 1986.
- [15] T.E. Springer, T.A. Zawodzinski, M.S. Wilson, S. Gottesfeld, in: S. Gottesfeld, G. Halpert, A. Landgrebe (Eds), Proceedings of the First International Symposium on Proton Conducting Membrane Fuel Cells I. The Electrochemical Society Proceedings, 1995, pp. 95–23.
- [16] T.E. Springer, S. Gottesfeld, in: R.E. White, M.W. Verbrugge, J.F. Stockel (Eds.), Proceedings of the Symposium on Modeling of Batteries and Fuel Cells. The Electrochemical Society Proceedings, 91-10, 1991, pp. 197–208.
- [17] C.H. Hamann, W. Vielstich, Electrochemie II, Verlag Chemie, Physik-Verlag, Weinheim, 1981.
- [18] A.A. Kornyshev, M.A. Vorotyntsev, Electrochim. Acta 26 (1981) 303.
- [19] D. Stauffer, A. Aharony, Introduction to Percolation Theory, revised 2nd ed, Taylor and Francis, London, 1994.
- [20] M.B. Isichenko, Rev. Mod. Phys. 64 (1992) 961.
- [21] Z. Ball, H.M. Phillips, D.L. Callahan, R. Sauerbrey, Phys. Rev. Lett. 73 (1994) 2099.
- [22] J.R. Macdonald (Ed.), Impedance Spectroscopy, Wiley, New York, 1987.
- [23] S.J. Lee, S. Mukerjee, J. McBreen, Y.M. Rho, Y.T. Kho, T.H. Lee, Electrochim. Acta 43 (1998) 3693.
- [24] V.A. Paganin, C.L.F. Oliveira, E.A. Ticianelli, T.E. Springer, E.R. Gonzales, Electrochim. Acta 43 (1998) 3761.